

Broadband, Single wavelength, Continuous Spectral Control in a Polymer-Based Solid-State Random Laser.

Bhupesh Kumar^{1,2}, Sebastian Schulz², and Patrick Sebbah^{1,*}

¹Department of Physics, The Jack and Pearl Resnick Institute for Advanced Technology, Bar-Ilan University, Ramat-Gan, 5290002 Israel.

²SUPA, School of Physics and Astronomy, University of St. Andrews, Fife, KY16 9SS, UK

*patrick.sebbah@biu.ac.il

ABSTRACT

In this paper, we present a study on partially pumped, single wavelength random lasing with tunability controlled by temperature in a solid-state random laser based on DCM (4-dicyanomethylene-2-methyl-6-(p-dimethylaminostyryl)-4H-pyran) doped PMMA (polymethyl methacrylate) dye. By carefully shaping the spatial profile of the pump, we achieve low-threshold, single-mode random lasing with excellent rejection of side lobes. Notably, we observe that varying the temperature induces changes in the refractive index of the PMMA-DCM layer, resulting in a blue-shift of the lasing wavelength. Moreover, we demonstrate continuous tunability of the lasing wavelength over an impressive bandwidth of 8 nm.

Introduction

Random lasers are unconventional laser sources in which feedback is provided by randomly-distributed scattering particles. In the past two decades, random lasers have been the subject of intense theoretical and experimental study [1-9]. Tunability and directionality are important features that determine the application scope of any laser device in fields such as integrated spectroscopy, remote sensing, and optical communication¹⁰. Spectral tunability in random lasers has been demonstrated via multiple mechanisms, including liquid crystal-based temperature-tunable random lasers¹¹, controlling the pump size and concentration of scatterers in a dye-doped polymer layer with air holes as scatterers in a two-dimensional configuration¹³, through varying the thickness of a gain medium consisting of silver nanoparticles embedded in dye-doped polymer¹⁴, selecting different dye molecules in a solution of metallic nano-particles^{15,16}, or mechanical stretching of a dye-doped polymer layer embedded with scatterers¹⁷⁻¹⁹. Other tuning mechanisms include engineered absorption of light emission²⁰, tunable plasmonic random laser based on switching to different order harmonic modes associated with different lengths of silver nanorods.²¹, temperature-controlled random laser in polymer optical fiber²², and electric-field-induced, wavelength-tunable random lasing in a liquid-crystal infiltrated disordered planar microcavity²³. However, most of these previous dye-doped polymer-based random lasers are limited to broad linewidth and multimode tunability.

Recently, we have demonstrated that, using an iterative pump shaping optimization method, selective excitation of a particular mode of the multimode emission spectrum and single-mode operation with high side-lobe rejection can be achieved^{9,24,25}. However, it is not possible to achieve lasing at any arbitrary desired wavelength, but only mode selection within the discrete multimode emission spectrum. It would be interesting to add tunability to this technique to achieve full spectral control in random lasers.

In this paper, we report single wavelength continuous broadband spectral tuning in a dye-doped solid-state random laser. Random lasers (RLs) typically produce multimode coherent light due to the random distribution of scattering particles. However, by using a combination of spatial pump shaping and the negative thermal coefficient of the refractive index of PMMA polymer, we are able to achieve single wavelength spectral control of a random laser on a single device. Specifically, we show continuous broadband tunability over a bandwidth of 8 nm.

Methods

Sample Preparation

Disorder structures were fabricated using e-beam lithography on a 600 nm layer of poly(methyl methacrylate) or PMMA that was doped with 5% weight of DCM (4-dicyanomethylene-2-methyl-6-(4-dimethylaminostyryl)-4H-pyran) laser dye. The fluorescence spectrum of the dye is centred around 600 nm, and it has a high fluorescence quantum yield and a large stoke

shift (100 nm), which means it does not reabsorb the emitted light. The PMMA used had a molecular weight of 49500 and was used at a concentration of 6% weight in anisole. The active, PMMA-DCM dye-doped polymer layer was obtained by

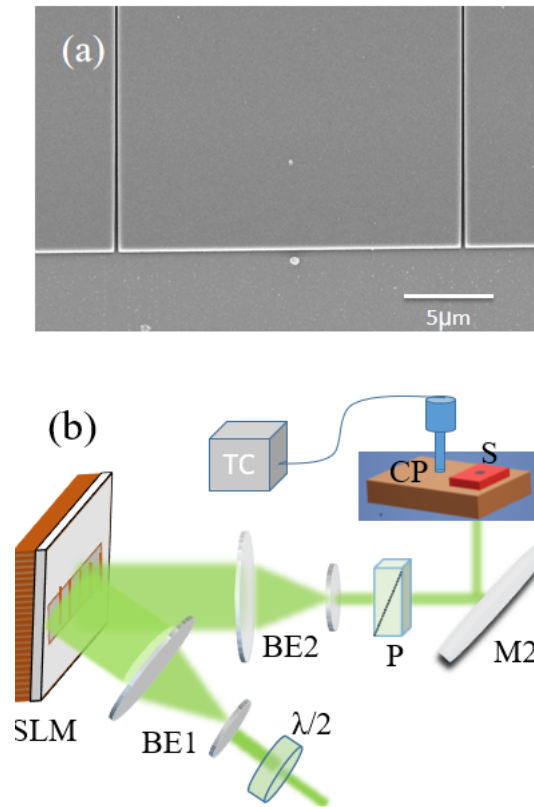


Figure 1. (a) High resolution SEM image of the small section of the sample from the top showing air grooves carved into the PMMA-DCM layer. (b) Schematic of the experimental setup. BE1 and BE2: Beam expanders; P: Polarizer, SLM: Spatial light modulator; M2: Mirror; S: Sample; TC: Temperature controller; CP: Copper plate;

spin-coating a doped-polymer solution at 1000 rpm for 60 seconds on a fused silica wafer (Edmund optics) and post baking it at 120°C for 2 hours in an oven²⁵. The silica wafer has a refractive index of 1.45, compared to 1.54 for the PMMA-DCM layer. To fabricate one dimensional(1D)-disorder samples, randomly distributed parallel 125 grooves, each on average 200 nm wide and 50 μm long, covering a total length of 1000 μm were carved into the PMMA-DCM layer using e-beam lithography (CRESTEC/CABL-9000C) (see Fig. 1(a)), resulting in dielectric sections with an average length of 8 μm separated by air gaps of 200 nm. The fabrication method ensures a high refractive index contrast of 0.54 between air grooves and the polymer layer, which helps in achieving random lasing action at a low threshold.

Experimental Setup

A schematic of the experimental setup is shown in Fig.1(b). The setup consists of a frequency-doubled mode-locked ND:YAG laser (EXPLA PL2230: 532 nm, 20 ps, maximum output energy 28 mJ, repetition rate 1-50 Hz). The beam is expanded 5X and spatially modulated by a 1952 x 1088 pixel reflective spatial light modulator (SLM) (Holoeye HES 6001, pixel size 8.0 μm). The SLM is placed in the object plane of a telescope with 4X reduction and is imaged on the sample. This setup is used to create a laser strip whose width and length are adjusted according to the sample dimensions. The disorder structure is precisely aligned with the laser strip line under a fixed stage Zeiss microscope (AxioExaminer A1) and imaged using an Andor Zyla sCMOS (22 mm diagonal view, 6.5 μm pixel size) CCD camera, using a 10X objective. The laser emission is collected through a multimode optical fiber connected to a Horiba iHR550 imaging spectrometer equipped with a 2400 mm^{-1} grating and Synapse CCD detection system (sampling rate 1 MHz, 1024 x 256 pixels, 26 μm pixel pitch). The entrance slit is 50 μm, resulting in a spectral resolution of 20 pm.

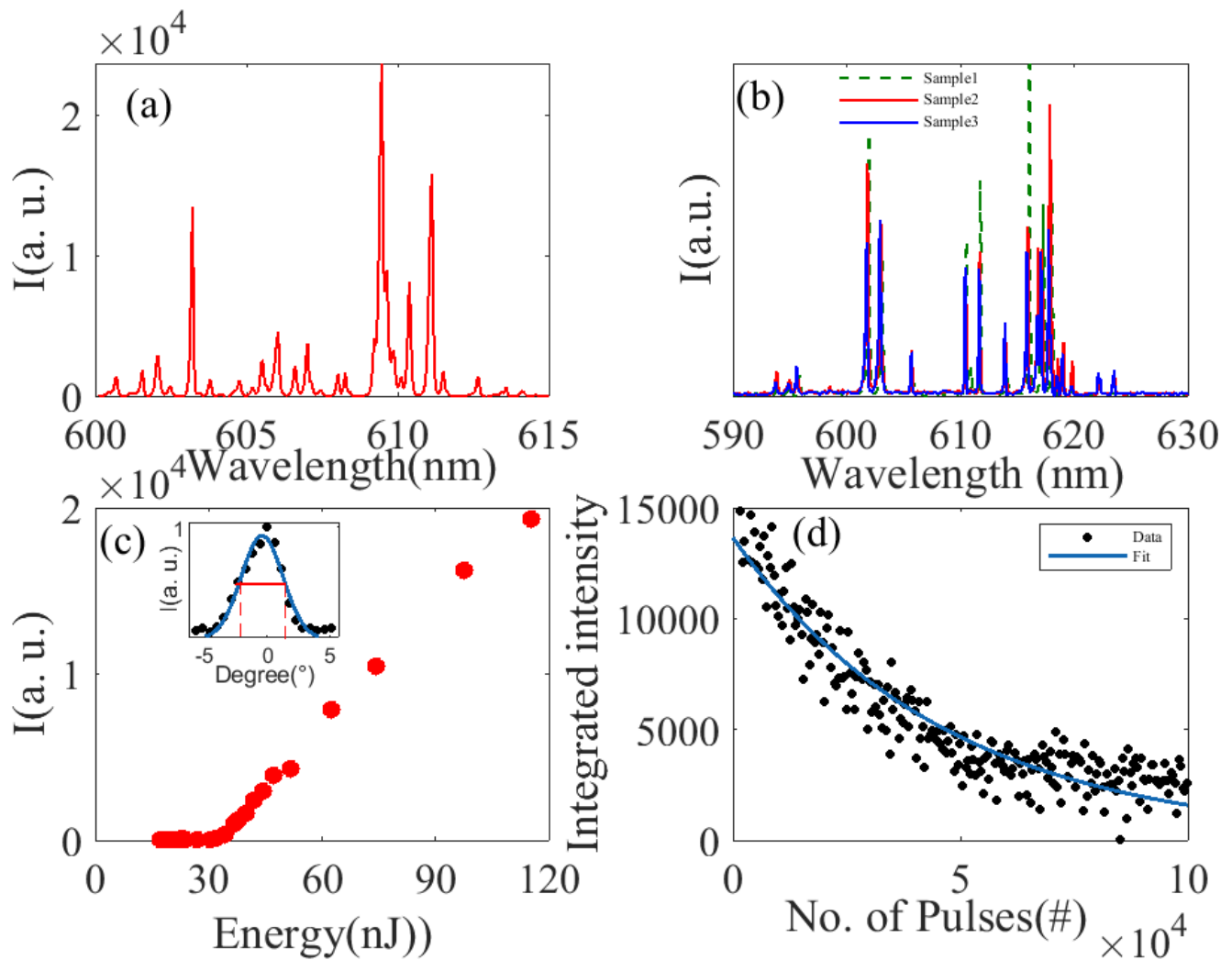


Figure 2. (a) Multimode Random laser emission spectra obtained after pumping the sample uniformly above the threshold, sample length $1000 \mu\text{m}$, pump size $1000 \mu\text{m} \times 50 \mu\text{m}$. (b) Emission spectra were recorded for 3 different samples of identical disorder configuration at same pump power. (c) The integrated intensity of the emission spectrum with increasing Pump energy (nJ). inset: Angular distribution of the integrated output intensity of random laser emission at a distance of 10 cm from the sample edge, the blue line is a Gaussian fit. (d) Integrated intensity as a function of the number of pump pulses for the random laser. The pump energy is about 50 nJ for a uniform pump of size $500 \mu\text{m} \times 50 \mu\text{m}$ at a repetition rate of 10 Hz. The blue line is an exponential fit.

Results

When the sample undergoes optical pumping, it experiences multiple scatterings of light through air grooves, creating enclosed optical loops. These loops generate the necessary resonances and coherent optical feedback, enabling the occurrence of random lasing with a narrow emission line width. Upon uniformly pumping the sample above the threshold, a multimode lasing spectrum is obtained (illustrated in Fig. 2(a)). The resulting spectrum displays randomly positioned, distinct lasing peaks, each exhibiting a typical linewidth of 0.2 nm, constrained by the resolution of the spectrometer.

Subsequently, we demonstrate the remarkable reproducibility of the disorder configuration in our random laser, which is attributed to the use of the highly precise e-beam nanolithography fabrication technique. To show spectral reproducibility, we manufacture three identical disorder configuration samples simultaneously on the same substrate. These samples are then subjected to uniform pumping at the same pump power, and their respective emission spectra are recorded. Remarkably, all three samples yield identical emission spectra, as depicted in Fig. 2(b).

Once the pump intensity reaches above the lasing threshold, the output intensity increases manifold. This nonlinear increase

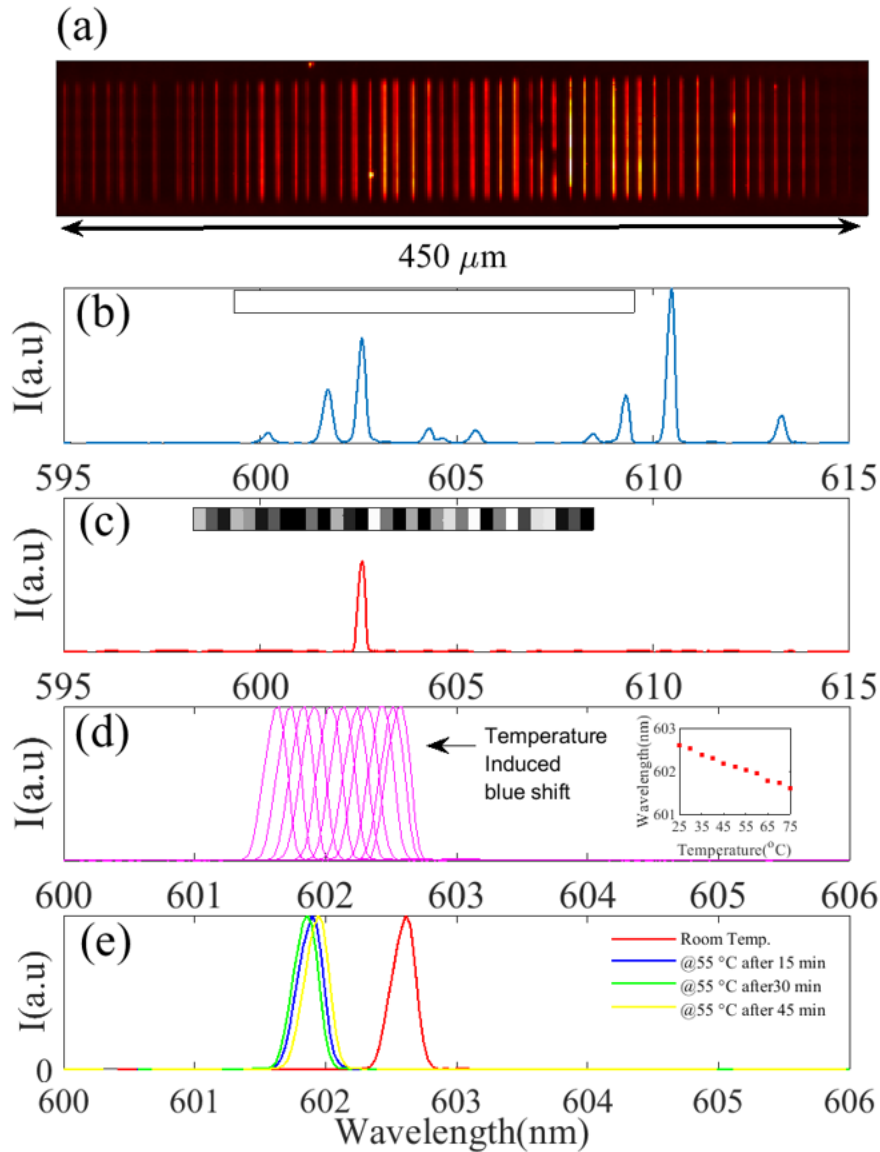


Figure 3. (a) Optical microscope image of field intensity distribution near the sample surface when pumped above the threshold. (b) Multimode emission spectra for a uniform pump strip of size $450 \mu\text{m} \times 50 \mu\text{m}$. (c) Singlemode lasing at $\lambda = 602.60 \text{ nm}$ after an iterative pump optimization process. Inset shows the optimized pump profile in gray scale. (d) The spectral blue shift of 1 nm in the single mode lasing spectrum at $\lambda = 602.60 \text{ nm}$ with increasing temperature of polymer layer. The figure in the inset shows the temperature vs wavelength plot. (e) Emission spectrum stability at constant temperature. The emission spectrum was recorded at an interval of 15, 30, 45 minutes when the sample is heated to constant temperature of $55 \text{ }^\circ\text{C}$.

in output intensity confirms the onset of random lasing action. By linear fit, the lasing threshold value is found to be 35 nJ for a pump size of $450 \mu\text{m} \times 50 \mu\text{m}$ (fig.1(c)). To find the directionality of emission from the sample edge in the x-y plane, the emission spectrum is collected by a 20X microscope objective coupled to a multimode fiber connected to a spectrometer. The microscope objective was placed at a distance of 10 cm from the sample edge and scanned to collect emission in a direction orthogonal to the sample length. Directional measurements are shown in inset Fig.2(c). Half of the emission intensity is confined within ± 2.5 degrees from the center of the sample.

We examined the photostability of our quasi-1D random laser by subjecting the sample to uniform pumping using the same experimental conditions as described earlier. The pump energy was held constant at 50 nJ, employing a pump size of $500 \mu\text{m} \times 50 \mu\text{m}$, and a pump laser repetition rate of 10 Hz. In Figure 2(c), we present the integrated emission intensity graphed against

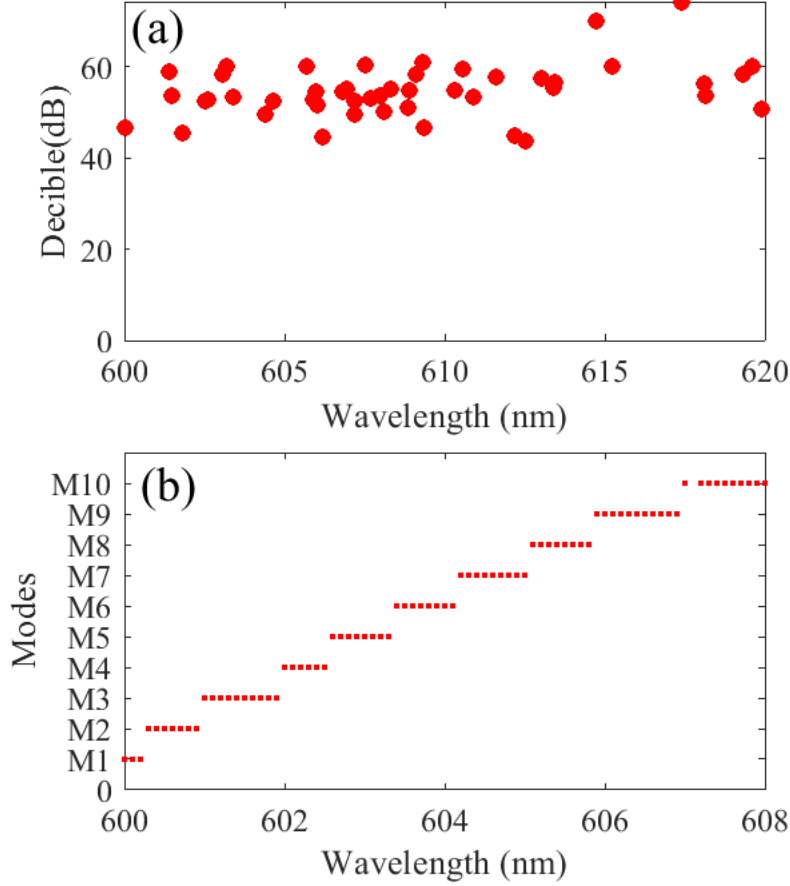


Figure 4. (a) Iterative optimization of pump shaping has been applied to select 50 lasing modes. The suppression ratio for each individually selected lasing mode w.r.t maximum noise count in the emission spectrum is plotted in log representation (dB). (b) Continuous tunability over a bandwidth of 8 nm by tuning of 10 different individually selected lasing modes M1= 601.2 nm, M2= 600.9 nm, M3= 602.50 nm, M4= 602.5 nm, M5= 603.3 nm, M6= 604.1 nm, M7= 605.00 nm, M8= 605.800 nm, M9= 606.900 nm, M10= 608.00 nm.

the laser pulse number. The photostability of the laser was observed to be 28380 pulses, equivalent to approximately 47.3 minutes, during which the integrated laser emission intensity reduced to half of its original integrated lasing intensity.

To achieve single mode lasing at any of the lasing wavelengths of the multimode emission spectrum(Fig.3(b)) We apply a nonuniform intensity profile to the pump beam by modulating the SLM. We implement an iterative optimization method^{9,25} to find the optimal pump profile for which modes other then the target mode are suppressed. Here we use Nelder-Mead simplex algorithm implemented in the fminsearch function of MATLAB to optimize the pump profile. We slightly modified the fminsearch function by setting the initial step (usually the δ parameter in fminsearch) to 1.0 in order to explore a larger region of the 32-dimensional space. The number of pixels (32) was chosen as a compromise between sensitivity and computation time. The Matlab-generated image that is sent to the SLM is made up of 32 intensity blocks, each of which is encoded on 256 levels of grey and projected onto the sample. To start the optimization process, we choose 32 column-vectors V_i from the 32 x 32 binary Hadamard matrix as the initial vertices.

The pump profile $P(x)$ is therefore written as

$$P(x) = \frac{1}{255} \sum_{i=1}^{32} \beta_i V_i$$

where β_i takes discrete values in the range [0,255]. Each vector β_i corresponds to a particular pump profile associated with a particular emission spectrum $I(\lambda)$. The optimization algorithm uses the inverse of the extinction ratio, $\eta = I_t/I_o$, as its cost function and aims for its minimization, where I_t is the peak intensity of the targeted mode and I_o is the highest intensity among all other modes except the targeted mode. To find the optimized pump profile, the algorithm iteratively generates a new pump profile, applies it to the pump stripe, acquires the emission spectrum averaged over 10 shots, and computes the cost function.

Mode selection and singlemode operation at the lasing wavelength of $\lambda = 602.60$ nm are achieved after the convergence of the iterative optimization, as shown in Figure 3(c). After 250 iterations, the algorithm converges to a pump profile that suppresses modes other than the targeted mode. The selected lasing mode has an extinction ratio(measured as the ratio of the peak intensity count of the target mode w.r.t. maximum noise level in the spectrum) of 800, corresponding to a sidelobe rejection of 53 dB. The next highest intensity count, except for the target mode, in the emission spectrum is 4 counts, which is close to the average noise level present in the spectrum.

Next, we demonstrate how the emission wavelength of the selected lasing mode can be tuned by changing the temperature of the sample. Our RL sample was positioned on a copper plate featuring a rectangular hole, slightly smaller in size than the sample. This arrangement facilitates the convenient placement of the sample over the hole, enabling us to pump the RL sample from the bottom. The copper plate is connected to a heating probe to heat the sample. A sensor is also connected to the copper plate to monitor the temperature. Figure 3(d) shows the blue shift of single-mode random laser emission initially centered at $\lambda = 602.60$ nm with a step size of 0.1 nm on increasing sample temperature in a step of 5 °C. We observed a total blue shift of 1 nm when the temperature of the sample increased from 25 °C to 75 °C. The inset in figure 3(d) shows the linear temperature dependence of the spectral shift. A linear fit gives a slope of $d\lambda/dT = -0.02$ nm/°C. When the sample cools down, back to 25 °C, the spectral shift follows the same path in the reverse direction. This behavior is easily explained by the fact that PMMA polymer has a negative thermal coefficient of refractive index^{26–28}. Its refractive index therefore decreases with increasing temperature, which results in a decrease in the optical path length within the polymer layer and a blue-shift. This process is reversible. The temperature-induced spectral shift can be applied to any wavelength of the multimode emission spectrum after selecting them individually using the iterative pump shaping optimization process. We also performed a spectral stability test at a constant temperature higher than room temperature in a minimum airflow lab environment. An optimally-pumped lasing sample emitting light @ $\lambda = 602.60$ nm is supplied with constant heat to achieve a wavelength shift of 0.60 nm at a sample temperature 55 °C. Then, the emission spectra are recorded at 3 intervals of 15 minutes each. Lasing emission at @ $\lambda = 602.00$ nm remains stable within ± 0.1 nm as shown in Fig.3(e). In our previous work, we showed that all the lasing modes excited under a uniform pump profile can be individually selected²⁵. First, we test the robustness of our pump profile optimization method to achieve a single lasing mode by selecting 50 different lasing modes on different samples. Figure 4(a) shows the sidelobe rejection of selected modes. All the modes are selected with an excellent side-lobe rejection of more than 40 dB.

To demonstrate continuous broadband tunability, we chose a sample of length 1000 μm with 125 air grooves. We explored different degrees of disorder by changing deviation from 0.1 μm to 3.5 μm from the mean periodic position of 8 μm . The goal was to identify a disordered pattern capable of lasing with 10-15 modes within 8 to 10 nm spectral bandwidth within the range of the spectral gain curve. A disorder pattern with a deviation of ± 0.5 μm around the mean periodic position of 8 μm yielded an average of 13 lasing modes within the wavelength range of 600 nm to 608 nm. We choose a pump length of 500 μm and run iterative optimization on different lasing modes in the spectrum, 10 lasing modes distributed over a wavelength range of 600-608 nm are individually selected by iterative optimization. The thermal-induced spectral shift was recorded for all the modes to achieve single-wavelength continuous broadband tunability over a impressive wavelength range of 8 nm (Fig.4(b)).

Discussion

In conclusion, our study showcases the successful implementation of iterative optimization of pump profiles and thermally-induced refractive index changes in dye-doped polymer layers, leading to the realization of single wavelength, broadband tunable random lasing in quasi-1D active disordered systems. The emission wavelength of any lasing mode individually selected using iterative pump shaping can be continuously blue-shifted by upto 1 nm when increasing the temperature of the PMMA-DCM layer. We envision that this thermally controlled, single-wavelength tunable random laser holds promising potential for future applications in on-chip wavelength tunable laser sources. The ability to precisely tune the lasing wavelength using thermal control opens new avenues for the development of compact and versatile on-chip laser devices with various practical applications.

Acknowledgement

We extend our heartfelt appreciation to Dr. Leonid Wolfson for his unwavering dedication to the lab, and to Dr. Yossi Abulafia for his valuable assistance with the fabrication process. We are grateful to the Bar-Ilan Institute of Nanotechnology and Advanced Materials for providing us access to their fabrication facilities. This research received generous support from The Israel Science Foundation through Grants No. 1871/15, 2074/15, and 2630/20, as well as from the United States-Israel Binational Science Foundation NSF/BSF through Grant No. 2015694 and No. 2021811. B. K. expresses gratitude to the PBC Post-Doctoral Fellowship Program from the Israeli Council for Higher Education. Additionally, P. S. acknowledges the support from the CNRS under grant PICS-ALAMO. B. K. and S. A. S. acknowledge funding from the Engineering and Physical Sciences Research Council (EPSRC[EP/V029975/1]).

References

1. H. Cao, Y. G. Zhao, S. T. Ho, E. W. Seelig, Q. H. Wang, and R. P. H. Chang Phys. Rev. Lett. **82**, 2278-2281 (1999).
2. C. Vanneste, P. Sebbah, Phys. Rev. Lett. **87**, 183903 (2001).
3. C. J. S. de Matos, L. S. Menezes, A. M. Brito-Silva, M. A. M. Gámez, A. S. L. Gomes, and C. B. de Araújo, Phys. Rev. Lett. **99**, 153903 (2007).
4. M. Gaio, D. Saxena, J. Bertolotti, D. Pisignano, A. Camposo, and R. Sapienza, Nat. Comm. **10**, 226 (2019).
5. J. Liu, P. D. Garcia, S. Ek, N. Gregersen, T. Suhr, M. Schubert, J. Mørk, S. Stobbe, and P. Lodahl, Nature Nanotechnology , **9** 285-289 (2014).
6. S. Schönhuber, M. Brandstetter, T. Hisch, C. Deutsch, M. Krall, H. Detz, A. M. Andrews, G. Strasser, S. Rotter, and K. Unterrainer, Optica, **3**,1035-1038 (2016).
7. DN. Dirin , RT. Lechner, G. Fritz-Popovski G,M. Sytnyk,S. Yakunin,S. Rotter , A. AAY, C. Vidal , C. Hrelescu, TA. Klar TA, MV. Kovalenko, W. Heiss, ACS Nano. **9**,9792-9801 (2015).
8. H. Liang, B. Meng, G. Liang, J. Tao, Y. Chong, Q. J. Wang, and Y. Zhang, Adv. Mater., **25**, 5859 (2013). B. Abaie, E. Mobini, S. Karbasi, et al. Light Sci Appl. **6**,17041 (2017).
9. N. Bachelard, S. Gigan, X. Noblin, P. Sebbah, *Nature Physics* **2014**, 10, 426-431.
10. D. Wiersma, The physics and applications of random lasers. *Nature Phys* 4, 359–367 (2008).
11. Q. Song, S. Xiao, X. Zhou, L. Liu, L. Xu, Y. Wu, and Z. Wang, Opt. Lett. **32**, 373-375 (2007)
12. Y. Chen; J. Herrnsdorf; B. Guilhabert; Y. Zhang; A. L. Kanibolotsky; P. J. Skabara; E. Gu; N. Laurand; M. D. Dawson. 2011 11th IEEE International Conference on Nanotechnology, 2011, pp. 559-563, doi: 10.1109/NANO.2011.6144325.
13. B. Kumar, R. Homri, and P. Sebbah. 2D tunable all-solid-state random laser in the visible., *Sci Rep* 13, 8337 (2023).
14. J. Tong, X. Shi, S. Li, C. Chen, T. Zhai, X. Zhang, *Org. Electron.*2019, 75, 105337
15. Ziegler, J.; Wörister, C.; Vidal, C.; Hrelescu, C.; Klar, T. A., *ACS Photonics* 2016, 3, 919.
16. Z. Wang, X. Meng, A. V. Kildishev, A. Boltasseva, V. M. Shalaev, *Laser Photonics Rev.*2017, 11, 1700212
17. T. Zhai, J. Chen, L. Chen, J. Wang, L. Wang, D. Liu, S. Li, H. Liu, and X. Zhang, *Nanoscale* 7(6), 2235–2240 (2015).
18. Y. Liao, Y. Lai, P. Perumal, W. Liao, C. Chang, C. Liao, S. Lin, and Y. Chen, *Adv. Mater. Technol.* 1(6), 1600068 (2016).
19. Y. Lee, C. Chou, Z. Yang, T. B. H. Nguyen, Y. Yao, T. Yeh, M. Tsai, and H. Kuo, *Nanoscale* 10(22), 10403–10411 (2018).
20. R. G. S. El-Dardiry and A. Lagendijk,
21. J. Zhang, F. Wang, S. Ghafoor, H. Wang, W. Zhang, K. Xie, R. Cheng, J. Yan, L. Niu, P. Wang, L. Zhang, Z. Hu *Adv. Opt. materials*, 10(10), 2200426 (2022).
22. Z. Hu, J. Xia, Y. Liang, J. Wen, E. Miao, J. Chen, S. Wu, X. Qian, H. Jiang, and K. Xie, *Opt. Express* 25, 18421-18430 (2017).
23. Q. Song, L. Liu, L. Xu, Y. Wu, and Z. Wang, *Opt. Lett.* 34, 298-300 (2009).
24. N. Bachelard, J. Andreasen, S. Gigan, and P. Sebbah *Phys. Rev. Lett.* 109, 033903
25. B. Kumar, R. Homri, Priyanka, S. K. Maurya, M. Lebental, and P. Sebbah, *Optica* 8, 1033-1039 (2021).
26. X.-l. Zhu and D. Lo, *J. Opt. A: Pure Appl. Opt.* 3 225 (2001)
27. F. J. Duarte and R. O. James, *Opt. Lett.* 28, 2088-2090, (2003).
28. F. J. Duarte, A. Costela, I. Garcia-Moreno, and R. Sastre, *Appl. Opt.* 39, 6522-6523 (2000)